Theoretical Chemistry Accounts (2018) 137:39
https://doi.org/10.1007/s00214-018-2223-2

REGULAR ARTICLE

The optical properties of adenine cation in different oligonucleotides: a PCM/TD-DFT study

Lara Martinez-Fernandez[1,2] · Aurora Muñoz-Losa[3] · Luciana Esposito[2] · Roberto Improta[1,2]

Received: 5 December 2017 / Accepted: 12 February 2018

Abstract

The absorption spectra of several systems containing an adenine (A) cation are computed in water by TD-DFT calculations, using three different functionals and including solvent effects by a mixed discrete–continuum approach. Our calculations well reproduce the experimental absorption spectrum of deoxyadenosine nucleoside cation (dA^+), which provides an intense peak at 350 nm and a weaker one at 600 nm, allowing its assignment. M052X and CAM-B3LYP predict that the hole is essentially localized on a single A base also in the cationic forms of dApdA dinucleotide, both in single and in double strand, and of (dApdT) duplex, exhibiting absorption spectra similar to that of dA^+. For all these compounds, B3LYP predicts instead the delocalization of the hole over two A bases. On this ground, it is possible to propose which would be the spectral signature of partial hole delocalization. Vertical and adiabatic ionization potentials for the compounds under investigation are also computed, providing values in good agreement with the available experimental results.

Keywords DNA · Hole delocalization · TD-DFT

1 Introduction

The generation of a cation, a 'hole', following absorption of light by a material is a key step in processes ranging from photovoltaic to photosynthesis [1, 2]. The study of the static and dynamic properties of photoinduced cationic species is thus of paramount importance for several research fields, such as material science [3, 4], electrochemistry [5] or biochemistry [6]. For what concerns the damage of the genetic code induced by UV light in DNA, recent studies have shown that for several oligonucleotides the absorption of a single photon at ~ 266 nm can ionize the base, with electron transfer to the solvent and formation of reactive radical species [7–11]. This process, besides having obvious biological consequences, is particularly puzzling, since the measured ionization potential (IP) of the purine nucleobases in water (7.3–7.7 eV) [12] is 2.5 eV larger than the energy deposited by 266 nm excitation (4.66 eV). On the one hand, it could be possible that some of the long living excited states created in oligonucleotides, such as those with significant charge Transfer (CT) [13–21] character, could be particularly prone to undergo ionization. On the other hand, it is also possible that inclusion of a base in the oligonucleotides leads to a dramatic lowering of the IP and that partial delocalization of the hole on multiple bases is possible [22–24]. The extent of hole localization in oligonucleotides is relevant also for the study of CT processes in DNA, which are critical to assess the possible use of oligonucleotides in optoelectronics, explaining the huge number of studies, both experimental and theoretical, focussing on charge transport in DNA [17, 22, 24–37]. In a series of interesting papers, Peluso and coll. examined several oxidized DNA sequences, ranging from oligoadenine single strand to guanine-rich fragments [38–41]. In oligoadenine single strands (containing up to

Published as part of the special collection of articles "Festschrift in honour of A. Rizzo".

Electronic supplementary material The online version of this article (https://doi.org/10.1007/s00214-018-2223-2) contains supplementary material, which is available to authorized users.

✉ Roberto Improta
robimp@unina.it

1 LIDYL, CEA, CNRS, Université Paris-Saclay, 91191 Gif-sur-Yvette, France

2 Consiglio Nazionale delle Ricerche, Istituto di Biostrutture e Bioimmagini, 80134 Naples, Italy

3 Área de Didáctica de las Ciencias Experimentales, University of Extremadura, Avda. de la Universidad, 10071 Cáceres, Spain

Published online: 26 February 2018

4 bases), the computed IP significantly decreases with the number of bases, mirroring a noticeable delocalization of the hole over multiples bases [38, 39]. For fragments containing stacked guanine bases, a similar result is found, though the decrease in the IP per base is significantly smaller than that found for adenine (A) [40]. In the present paper we study the possible hole delocalization from a different perspective, focussing on the study of the electronic absorption spectra of A cation. We compare the results obtained for the isolated base in water with those of larger fragments, namely A dinucleotide (dApdA, hereafter $(dA)_2$) both in single and in double strands, and $(dAT)_2$ duplex. Transient absorption spectroscopy is the basic tool to characterize the cascade of chemical processes triggered by ionization. Adenine cation (A^+) is indeed instable with respect to deprotonation at the amino group (A-H6 radical, Scheme 1), but this reaction is sensitive to environmental effects (pH, temperature, etc.) [42–44]. Furthermore, recent studies show that for isolated dA the absorption spectra of the two radicals (A^+ and A-H6) are extremely similar [7]. An accurate analysis of the spectral changes induced by the inclusion of A^+ into the oligonucleotides is fundamental to interpret the time-resolved spectra obtained after one photon ionization, especially considering that these spectra could be significantly sensitive to partial hole delocalization. Conversely, we also aim to look for a spectral signature of the hole delocalization, which would be extremely useful to characterize the charge migration processes in DNA. This study also provides the opportunity to get additional insights on the effects ruling hole localization/delocalization in DNA and, finally, to better assess the performance of different TD-DFT functionals in reproducing the absorption spectra of open shell species.

2 Computational details

2.1 Quantum mechanic calculations

The ground state of the neutral and cationic species was optimized using density functional theory (DFT), comparing the performance of three different functionals, B3LYP [45], CAM-B3LYP [46], and M052X [47, 48]. Solvent effects were taken into account implicitly by considering the polarizable continuum model (PCM) [49, 50] and in specific cases also explicitly including a small number of water molecules of the first solvation shell into the calculations (see Scheme 1). When computing the vertical ionization potential (VIP) of dA, we have considered dynamic solvation effects by using state-specific [51] PCM calculations, which have been shown to provide values close to experimental IPs for several nucleobases [12, 52, 53]. The absorption spectrum at each minimum was simulated by computing the vertical absorption energies (VAE) using the time-dependent version of DFT (TD-DFT). Each VAE was convoluted using a gaussian function with half width at half maximum = 0.4 eV. Formal charges have been estimated by a Mulliken population analysis in terms of δq, i.e., the difference between the populations of purine ring in the cation and in the neutral ground state. Geometry optimizations have been performed by using the 6-31G(d) basis set, ionization potentials and the VAEs by performing 6-31 + G(d,p) single-point calculations. This has been the reference level of calculation for this study. Single-point calculations on dA have also been performed by using the 6-311 + G(2d,2p) basis set. Gaussian 09 package was used for all the QM calculations [54].

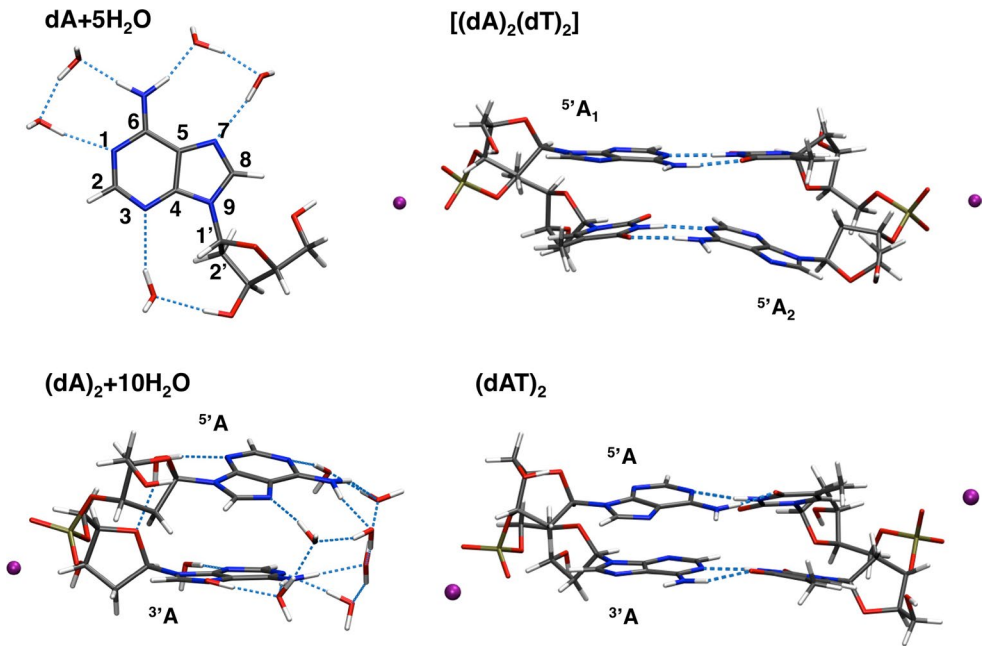

Scheme 1 Representation of the systems under study. See dA for atom labelling and the position of explicit water molecules

2.2 Molecular dynamic simulations

The $(dA)_5$ single helix was built in JUMNA software [55] and subjected to 500 ns molecular dynamics (MD) simulation performed by the Amber 11 suite of programs [56] with the bsc0 [57] modification to the parm99 force field [58]. The $(dA)_5$ structure was solvated with SPC/E water model [59] in a truncated octahedral box using a 11 Å distance between the solute and the edges of the box. The system was neutralized with K^+ counterions, and an excess of KCl was added to achieve a final concentration of ~ 150 mM. Periodic boundary conditions were used, and electrostatic interactions were treated using the particle mesh Ewald methodology with a cut-off value of 9 Å. Lennard–Jones interactions were truncated at 9 Å. Equilibration was performed using previously published protocols [60–62]. The production simulation was run in the *NPT* ensemble at 300 K using the Berendsen algorithm for temperature and pressure control (coupling time set to 5 ps). SHAKE constraints [63] were applied to all bonds involving hydrogen atoms, allowing for a stable simulation with a 2-fs integration time step. The atomic coordinates were saved every 1 ps along the production trajectory. From the latter, snapshots were extracted every 5 ns, for a total of 100 structures. In order to minimize the effects coming from the terminal 5′- and 3′-end nucleosides, we considered the central dimer (A3–A4) in the $(dA)_5$ structures selected by using it in the subsequent quantum calculations. The VIPs were computed without the counterion and explicit water molecules.

3 Results

3.1 dA monomer

3.1.1 Ionization potential

The computed VIP for dA in solution (taking into account dynamical solvation effects) is 7.4–7.7 eV, (depending on the selected functional, Table 1), which is in good agreement with the experimental results (7.6 eV for AMP) [12] and previous computational studies (7.7 eV) [12, 52, 64]. Including solvent effects significantly lowers the VIP compared to gas phase, [12, 52, 64–66]; on the other hand, explicit inclusion of water molecules has a limited effect on the VIP and negligible on the adiabatic ionization potential (AIP), in line with previous studies [52]. Linear response PCM shows once again its limitations in the treatment of dynamical solvation effects, providing severely underestimated VIP values [12, 52, 53, 64, 67, 68].

Confirming the results obtained on DNA bases [53], M052X provides the VIP values closest to the experimental estimates; CAM-B3LYP also is sufficiently accurate, whereas the B3LYP results are underestimated by 0.3 eV with respect to the experimental ones.

The cation is essentially localized over the purine ring ($\delta = 0.9$ a.u.) according to a simple Mulliken population analysis (see computational details). The charge delocalized on the sugar atoms is very small ($\delta = 0.1$ a.u.), the largest contribution coming from $C1'$ (0.022) and $C2'$ (0.025) carbon atoms.

3.1.2 Absorption spectra

The experimental absorption spectrum of A^+ in LiCl glass exhibits a broad band at ~ 600 nm (Band I in the following) and a more intense peak at ~ 340 nm (Band II in the

Table 1 Vertical and adiabatic ionization potential (VIP and AIP in eV) for the different systems computed at the specified functional combined with the 6-31 + G(d,p) basis set

	VIP			AIP		
	B3LYP	M052X	CAM-B3LYP	B3LYP	M052X	CAM-B3LYP
dA gas phase	7.94	8.16	8.07	7.59	7.77	7.69
dA	7.46 (6.37)	7.68 (6.58)[a]	7.60 (6.49)	6.10	6.32[b]	6.19
dA + $5H_2O$	7.42 (6.37)	7.76 (6.70)	7.56 (6.50)	6.14	6.38	6.23
$(dA)_2$	7.16 (6.28)	7.65 (6.77)	7.55 (6.71)	6.08	6.31	6.21
$(dA)_2$ + $10H_2O$	7.20 (6.34)	7.67 (6.84)	7.65 (6.79)	6.21	6.50	6.35
$(dAT)_2$	6.97 (6.20)	7.50 (6.78)	7.48 (6.69)	6.11	6.27	6.19
$[(dA)_2(dT)_2]$	6.98 (6.19)	7.53 (6.63)	7.43 (6.59)	6.13	6.29	6.19

Solvent effects considered with PCM (and including explicit water molecules if specified). VIP computed at the state-specific non-equilibrium level (the linear response results are reported in parenthesis)

[a]6.58 eV with the 6-311 + G(2d,2p) basis set

[b]6.33 eV with the 6-311 + G(2d,2p) basis set

following), ca. three times more intense than the red wing feature (inset in Fig. 1) [7]. The spectrum of A^+ in water solution at room temperature is not available, due to the larger stability of A-H6 radical, whose spectrum in water, however, is extremely similar to that recorded in LiCl glass [7].

The computed spectrum (Fig. 1) of dA^+ is fully consistent with the experimental one for all the density functional examined, with two bands, a broad one at ~ 600 nm (Band I = 2.07 eV) and a more intense peak at ~ 340 nm (Band II = 3.65 eV). From the quantitative point of view, B3LYP provides a spectrum which is blue-shifted by 0.2 (Band I) and 0.5 (Band II) eV with respect to the experimental one, while the blue-shift with respect to the experiments increases at the CAM-B3LYP (0.4 and 0.7 eV for Band I and Band II, respectively) and M052X level (0.5 and 0.6 eV for Band I and Band II, respectively). On the other hand, our calculations lack of vibrational and thermal effects, whose inclusion is expected to induce a significant red-shift (~ − 0.2 eV) of the computed spectrum [69, 70]. Considering the effect of an additional increase in the basis-set size, the PCM/TD-B3LYP spectrum would result extremely close to the experimental one, whereas those provided by CAM-B3LYP and M052X would be moderately blue-shifted, by 0.2 and ~ 0.3 eV respectively. The relative intensity of two bands is instead well reproduced by all the functionals employed.

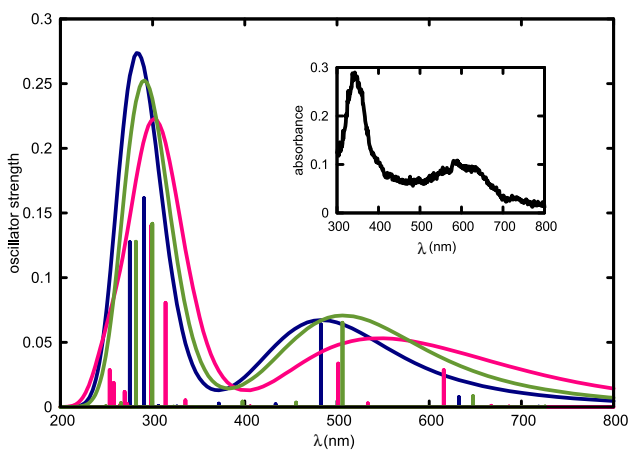

Fig. 1 Spectrum of dA^+ monomer computed in PCM at the B3LYP/6-31 + G(d,p) (pink), M052X/6-31 + G(d,p) (blue) and CAM-B3LYP/6-31 + G(d,p) (green) levels of theory. Inset: experimental spectra extracted from ref [7]

Several transitions, some of them weak, contribute to the absorption spectra. The most intense transition, being the main responsible of Band II corresponds to a SOMO → LUMO α excitation, and it is reminiscent of the HOMO → LUMO state of the parent neutral A. Band I can be assigned to transitions involving β spin and SOMO orbital, being two of them relatively more intense than the others (at ~ 500 nm and > 600 nm). According to B3LYP, these two transitions have similar intensity, whereas according to M052X and CAM-B3LYP the one at 500 nm is much more intense. This feature explains why the shape of the M052X and CAM-B3LYP spectra is closer to the experimental one; at the B3LYP level Band I is broader than its experimental counterpart.

The qualitative assignment of the electronic transitions is similar for all the functionals examined (Table 2). However, the M052X and B3LYP orbitals are different, with the latter functional providing larger contributions from orbitals mainly localized over the sugar ring (see Fig. 2). We have also observed such larger participation of the sugar moiety (and even H_2O molecules) in B3LYP orbitals for the $(dA)_2$ system. Inclusion of explicit solute–solvent hydrogen bonds does not dramatically affect the absorption spectrum, except for a small increase of the intensity of Band I and a tiny red-shift of Band II (Figure S1).

3.2 $(dA)_2$ dinucleotide: single strand

Once having optimized the minimum for $(dA)_2$ starting from a B-DNA conformation, we have computed the VIP and then the AIP, following $(dA)_2^+$ optimization at the PCM/DFT/6-31G(d) level, by using the three functionals examined. When computing the VIP, all functionals predict that the hole is delocalized, though not perfectly, on the two bases: δq-$^{5'}$A 0.53, 0.57 and 0.39 and δq-$^{3'}$A 0.38, 0.36 and 0.53 a.u. at M052X, CAM-B3LYP and B3LYP levels, respectively. The picture provided by the three functionals is instead dramatically different after geometry optimizations of $(dA)_2^+$. Both M052X and CAM-B3LYP predict indeed that the extent of

Table 2 Assignment, vertical absorption energies (VAE, in eV [nm]) and oscillator strengths (*f*) for the first four transitions calculated for dA^+ in PCM using different functionals and the 6-31 + G(d,p) basis set

	B3LYP		M052X		CAM-B3LYP	
	VAE	*f*	VAE	*f*	VAE	*f*
Hβ → S	2.01 [615]	0.029	2.57 [482]	0.064	2.45 [506]	0.065
$\pi\beta$ → S	2.47 [501]	0.034	3.33 [371]	0.003	3.12 [397]	0.004
S → Lα	3.95 [313]	0.081	4.27 [290]	0.162	4.14 [300]	0.142
$\pi_2\beta$ → S	4.16 [298]	0.140	4.51 [275]	0.127	4.40 [282]	0.128

The MOs most involved in each transition are shown in Fig. 2. S stands for SOMO orbital

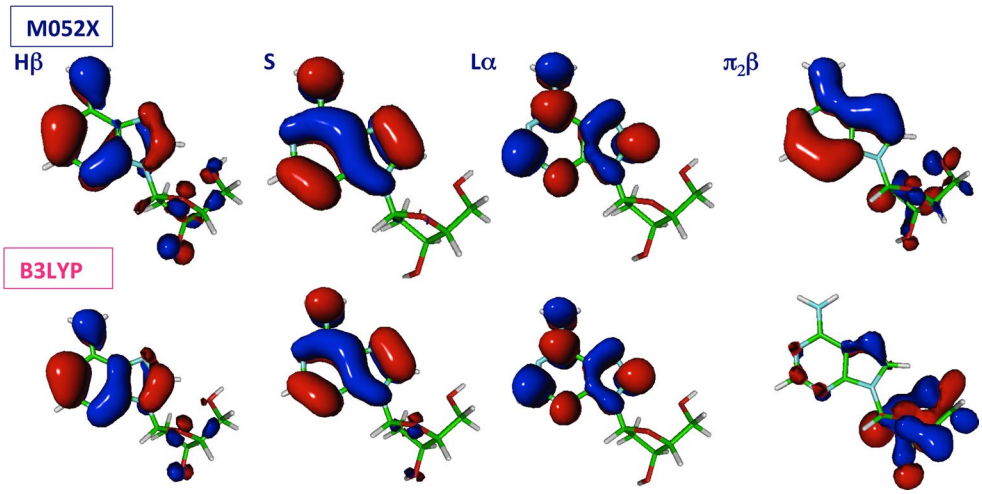

Fig. 2 Molecular orbitals of dA^+ involved in the most intense transitions collected in Table 2

hole delocalization is rather small, though not exactly zero. In $(dA)_2^+$ minimum the two A bases exhibit very different geometries: one is very similar to a neutral A, while the other to the A^+ cation. Accordingly, Mulliken population analysis shows that ~ 85 to 90% of the extra charge is localized over one $^{3'}$A ring while the remaining 15–10% is distributed on the backbone. Analysis of the spin density provides the same conclusion. As shown in Fig. 3, the unpaired electron is essentially localized over one A and, therefore, the hole in the other.

As shown in Table S1 and Figure S4, A ionization leads to noticeable structural changes in the dinucleotide: (i) the χ angle of the two bases shifts up to 30–40°, (ii) the phase angle of the $^{3'}$A increases, and (iii) the stacking area between the two bases decreases. These shifts can be explained by the tendency of the cationic base to partially unstack in order to be better exposed to the solvent.

B3LYP calculations predict instead that the hole is fully delocalized over the two bases, which are characterized by geometrical parameters intermediate between those typical of A and A^+. According to Mulliken population analysis, δq is 0.43 a.u for $^{5'}$A and 0.47 a.u. for $^{3'}$A, and the unpaired electron is delocalized on the two bases (see Fig. 3).

The vertical and adiabatic IPs of $(dA)_2$ are collected in Table 1. The computed SS-PCM VIP for $(dA)_2$ exhibit a small decrease (^{M052X}0.03 and $^{CAM\text{-}B3LYP}$0.05 eV) with

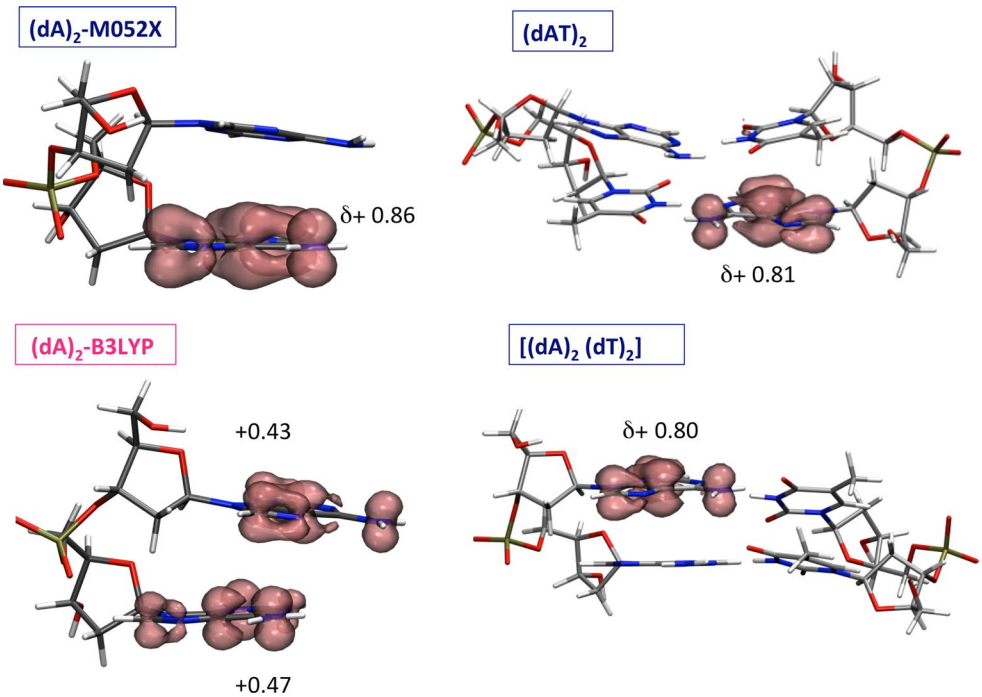

Fig. 3 Spin densities and δq values for the optimized cationic species of $(dA)_2^+$ and duplexes, using the specified functionals (M052X in blue and B3LYP in pink)

respect to the values computed for dA. Differences between dA^+ and $(dA)_2^+$ AIPs are even smaller, decreasing by 0.01 eV at M052X and increasing by 0.02 eV at CAM-B3LYP. This result is not surprising because, when going from dA^+ to $(dA)_2^+$ the extra stabilization of the cation (which is possible only in the dinucleotide) can be counterbalanced by the larger exposure to the solvent experienced by the monomer.

Indeed, the shifts predicted for the AIP are very small also for B3LYP, notwithstanding the extreme hole delocalization predicted by this functional. For CAM-B3LYP and M052X, the computed AIP does not remarkably depend on the inclusion of explicit solvent molecules, in agreement with previous studies for A [52]. On the other hand, for B3LYP inclusion of explicit H_2O has a dramatic effect on the final picture, since it leads to a localization of the cation at the $^{5'}$A base, with δq equal to 0.72 a.u.

As a last step of our analysis of the effects modulating the IP in longer sequences, we have investigated the role of conformational flexibility on the VIP. To this aim, we have computed the VIP for 100 different dimer structures extracted from a long MD simulations on $(dA)_5$ pentamer, as explained in the Computational Details section. The average value obtained from 100 configurations at the PCM/M052X/6-31 + G(d,p) NEQ level is 7.54 ± 0.11 eV, i.e., 0.08 eV lower than that obtained for $(dA)_2$ after geometry optimizations at the same level of theory. VIPs values span a range of 0.5 eV (from 7.30 to 7.80 eV). In order to check if this result is due to the use of geometries issuing from MD simulations, we also calculated the VIPs of all the A structures in the dimers as isolated monomers (200 calculations in total). In this case PCM/M052X/6-31 + G(d,p) gives an average VIP of 7.74 ± 0.11 eV, i.e., 0.2 eV larger than that found for the dimers, confirming that inclusion of conformational disorder leads to a slight decrease of the VIP.

The absorption spectra computed for $(dA)_2^+$ by the three density functionals are collected in Fig. 4 together with their $(dA)^+$ monomer counterpart. For M052X the absorption spectrum is very close to that predicted for $(dA)^+$, with band maxima almost superimposed and the relative intensity of Band I and II maintained (Fig. 4a). The most intense transitions are not significantly affected by the extremely small hole delocalization (δq is 0.85 for $^{3'}$A) and are very similar to those described above for A^+. The only noticeable difference concerns the lower intensity of the $(dA)_2^+$ spectrum compared to the monomer, which is likely due to the presence of the 'neutral' A stacked to A^+. This base, besides decreasing the solvent exposed surface of A^+, provides a small contribution to the A^+ transitions, which could give account of their rather low intensity. The presence of a close lying stacked A base also induces the appearance of several almost dark low-energy transitions, involving interbase excitations. For example, the lowest energy excited state (falling at 1.2 eV) basically involves hole transfer from the cationic A to its stacked partner. These transitions, which, because of their very small oscillator strength, do not noticeably affect the absorption spectra, could, nonetheless, modulate the photophysics of A^+ containing sequences. Furthermore, it is also possible that, because of the conformational fluctuations of oligonucleotides, for some structural arrangements the intensity of these dark transitions could increase, leading to a broadening of Band I with respect to that found in dA^+. For CAM-B3LYP, where the degree of localization is even larger (δq is 0.9 for $^{3'}$A), the spectra of $(dA)_2^+$ and the monomer are very similar and the decrease in the intensity with respect to the monomer is less significant than for M052X.

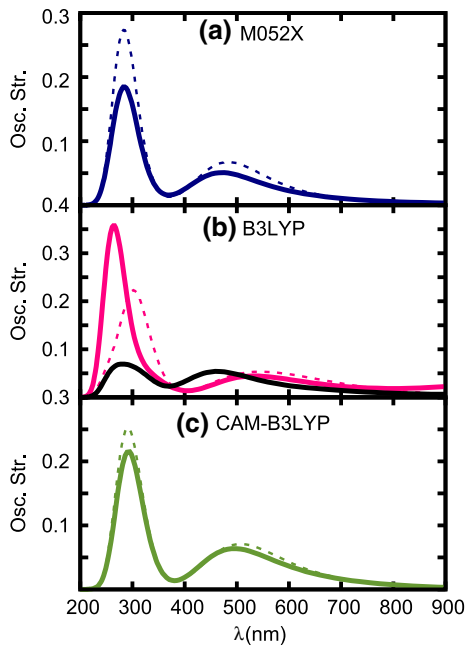

Fig. 4 Spectrum of $(dA)_2^+$ (solid) and dA^+ monomer (dashed) computed in PCM at the **a** B3LYP/6-31 + G(d,p) (pink), **b** M052X/6-31 + G(d,p) (blue) and **c** CAM-B3LYP/6-31 + G(d,p) (green) levels of theory. In panel **b** the spectra computed at the M052X/6-31 + G(d,p) for the optimized $(dA)_2^+$ B3LYP/6-31G(d) minimum is shown in black solid line

The spectrum computed for $(dA)_2^+$ by B3LYP is instead very different from that of dA^+, with a broad red tail in the visible appearing in the spectrum (Figs. 4b and S2). On the other hand, the analysis of the electronic transitions reveals that most of the low-lying excited states have a significant CT character. B3LYP suffers indeed from the well-known limitations of non-long-range corrected functionals and hugely overestimates the stability of long-range CT transitions [71]. Actually, in the system $(dA)_2^+ \cdot 10H_2O$, a very broad band in the visible is present, where many transitions have a solute–solvent CT character, often involving one base and the solvation shell of the other one (see Figure S3). The presence of many spurious low-energy CT transitions makes very difficult to use the B3LYP results to investigate the

consequences of hole delocalization on the optical spectra. To this aim, we have computed the spectra of $(dA)_2^+$ at the PCM/TD-M052X level, but using the minimum optimized at the B3LYP level, where the two bases have very similar geometries. The hole appears to be more delocalized than when using the M052X optimized geometry, though it is clear that the unpaired electron is mainly localized over the $^{5'}$A. This partial delocalization has a dramatic effect on the absorption spectrum. The red wing tail is significantly more intense, leading to the broadening of Band I, while the relative intensities of Band I and Band II are much more similar (Fig. 4b).

3.3 Duplexes

In the alternated AT sequences, the structural properties of the cation, $(dAT)_2^+$, are similar to those found in isolated dA^+; this result could be expected since the IP of Thymine is larger than that of A, explaining why the hole is essentially localized over this latter base, as shown in Fig. 3. Mulliken population analysis, accordingly, indicates that δq is 0.81 for one A and 0.11 for its associated backbone (with the C atom of the sugar bonded to A showing $\delta q = 0.02$ a.u). As a consequence, the absorption spectrum predicted in the duplex is very similar to that found in the monomer (Fig. 5a), for what concerns both the position and the intensity of Band I and Band II. SS-NEQ-VIPs are slightly lower (~ 0.2 eV) for $(dAT)_2$ compared to the monomer; on the other hand, the computed AIPs are very similar to those of dA^+ (Table 1). B3LYP predicts instead that the hole is delocalized over the two bases (δq is 0.40 for $^{5'}A_1$, and δq is 0.44 for $^{5'}A_2$), notwithstanding the poor stacking between the two bases. Actually, in $(dAT)_2^+$ hole delocalization leads to a significant decrease of the adenine interbase distance (Figure S5).

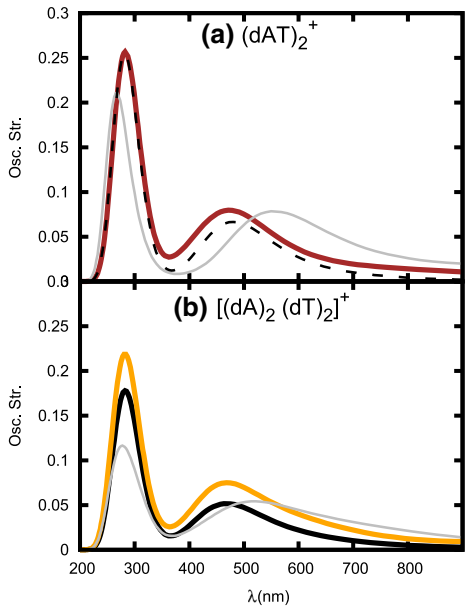

Fig. 5 Spectrum of **a** $(dAT)_2^+$ (brown) and dA^+ monomer (black dashed) and **b** $[(dA)_2(dT)_2]^+$ (yellow) and $(dA)_2^+$ dimer (black) computed in PCM at the TD-M052X/6-31G(d) level of theory. The spectra computed on the PCM/B3LYP/6-31G(d) minima are shown in grey

In AT homoduplex $[(dA)_2(dT)_2]^+$, we observe instead a scenario rather similar to what found for $(dA)_2^+$. Within the duplex, the two A are not as close as in $(dA)_2^+$; for example, the interbase distance $^{3'}C4$–$^{5'}C2$ is ~ 0.3 Å larger (3.45 and 3.17 Å, respectively). Also in $[(dA)_2(dT)_2]^+$ the hole is almost perfectly localized over one of the two A bases ($^{5'}$A), as shown by the spin density (Fig. 3), and by $\delta q = 0.80$. On the other hand, the presence of a stacked A affects the electronic transitions, whose positions are very similar to those of dA^+, but whose intensity decreases, as discussed above for $(dA)_2^+$ (Fig. 5a, b). Inspection of the transition densities shows indeed that some of the most intense transitions acquire a small intra-strand CT character. The decrease is smaller for $[(dA)_2(dT)_2]^+$ compared to $(dA)_2^+$, probably due to the larger interbase distance observed in the duplex. As for $(dA)_2^+$, B3LYP predicts hole delocalization over the two A bases (δq is 0.38 for $^{3'}$A and δq is 0.46 for $^{5'}$A).

Also for duplexes we have exploited the availability of minima presenting hole delocalization to gain insights into the consequences of this phenomenon on the optical spectra, by means of PCM/TD-M052X calculations on the PCM-B3LYP minima. For both $(dAT)_2^+$ and $[(dA)_2(dT)_2]^+$ duplexes, the spectra of the delocalized cation, plotted in grey in Fig. 5, show that the relative intensity of Band I increases, confirming the indications obtained on $(dA)_2^+$. A small red-shift of Band I maximum is also observed.

Also for the homoduplex our calculations predict a small decrease of the IP, with respect to the monomer (~ 0.15 eV), whereas the AIPs are not affected. The small shift found in the VIP does not depend on hole delocalization: we find indeed very similar results in the alternated and in the homoduplex. A larger computational model would be necessary to assess the effect of DNA on the VIP of A. Interestingly, the ionization process does not induce striking changes in the stacking geometry, but, as expected, the presence of the cation strengthens one of the WC hydrogen bonds.

4 Concluding remarks

In this study we have analysed the optical properties of the cation derivative of A nucleoside in different environments, from the aqueous solution to a dinucleotide, both in single and in double strands. In the former case, we studied the AA sequence, whereas in the latter both the AA and the AT sequences. We resorted to DFT and TD-DFT calculations,

checking the performances of three commonly used density functionals, namely B3LYP, CAM-B3LYP and M052X. Aqueous solution was described by the polarizable continuum model and, for dA and $(dA)_2$, including up to ten water molecules of the first solvation shell. Our aim was to verify the possibility of partial hole delocalization and, if this was the case, its consequences on the spectrum. The calculation of the spectra was also complemented by the computation of vertical and adiabatic ionization potentials.

For $(dA)^+$ all the adopted functionals provide an absorption spectrum in qualitatively agreement with the experimental one, which enables the assignment of the two most intense bands appearing in the spectrum at ~ 600 nm (Band I) and at ~ 340 nm (Band II). The former is due to two transitions involving the β electrons, and, in particular, the SOMO. Both α and β electrons instead contribute to Band II. The computed VIP is very close to the experimental one, M052X being the most accurate between the functionals examined. It is confirmed that a proper inclusion of dynamical solvation effect is mandatory to reproduce the vertical ionization potential in solution.

Both CAM-B3LYP and M052X predict that the hole is essentially localized on the purine ring of a single A base also in dinucleotides, not only in the presence of a T but also when two A bases are stacked. As a consequence, the spectrum of the cation is very similar to that computed for $(dA)^+$. Consequently, also the VIP and AIP are very similar to those predicted for the monomer. Recent studies have instead shown that partial hole delocalization in stacked adenines can decrease the IP up to 0.2 eV [38, 39]. On the other hand, these estimates have been obtained for A^+ embedded within a single strand, i.e., for a model of the monomer very different with respect to that examined here. In our case, instead, the larger solvent exposed surface in the monomer can counter-balance the possible hole delocalization effect. Actually, the comparison between the stacking geometry of $(dA)_2$ and $(dA)_2^+$ confirms that ionization can induce a small, but noticeable unstacking, allowing a better exposure of the cation to the solvent.

Also B3LYP predicts the IPs of dA and $(dA)_2$ are similar, notwithstanding this functional predicts that the hole is delocalized over two A. Analysis of the cations of AT and AA duplexes provides the same conclusion drawn for the single strand, with B3LYP predicting a full hole delocalization over the two A bases, also for (dAT) alternated duplex, where the stacking between the A bases is poor. Rapid deprotonation of A cation in oligoAde single strand does not allow to get unambiguous experimental indications on the possible hole delocalization [7]. On the other hand, following UV absorption, transient IR spectra of alternated and homo AT duplexes show the spectral signature of A cation, which is formed on a < 5 ps timescale and decays back to the ground state within 300 ps, without any hint of significant hole delocalization [15]. This result suggests that B3LYP has a tendency to over-stabilize delocalized cationic electronic structures and confirms that the description of localization/delocalization is extremely sensitive to the adopted computational model and, for DFT calculations, to the chosen functional. For what concerns solvent effect, inclusion of explicit solute–solvent hydrogen bonds favours hole localization.

A single-point TD-M052X calculation on the minimum of $(dA)_2^+$ computed by B3LYP gives useful insights on the consequences of hole delocalization on the optical spectra of dA^+ cation. In the presence of a partial delocalization, the relative intensity of Band I and Band II is more similar, and intensity of the broad red tail for $\lambda > 700$ nm increases.

The picture just described is that issuing from the analysis of the minima, which, though representative of highly populated regions of the potential energy surface (for example, the B-DNA conformation), could not provide an exhaustive description of the conformational behaviour of DNA, especially for single strand. As a first step towards the inclusion of conformational fluctuations [72] in our treatment, we have computed the VIP of a $(dA)_2$ on an ensemble of structures issuing from a long MD simulation of an oligoAde fragment. This procedure indicates that the VIP decreases by ~ 0.2 eV with respect to that found for the monomer; strand fluctuations, allowing, for example, closely stacked bases or the approach of the negatively charged phosphate moiety to one of the base, can thus modulate DNA photoionization. Analogously, for what concerns AIP, it could be in principle possible that starting from peculiar strand conformations, geometry optimizations lead to partially delocalized A cations. On the other hand, our results point out a strong tendency to localize the hole on a single A base.

Acknowledgements The authors thank CNRS-CNR PICS project (No. 6827-2015)/Bilateral CNR/CNRS for financial support. R.I. thanks the Université Paris-Saclay (Chaire d'Alembert No. 2016-10751). L.M-F thanks the 'OSPEG' LABEX PALM project.

References

1. Ponseca CS, Chábera P, Uhlig J, Persson P, Sundström V (2017) Ultrafast electron dynamics in solar energy conversion. Chem Rev 117(16):10940–11024
2. Barber J, Tran PD (2013) From natural to artificial photosynthesis. J R Soc Interface 10(81):20120984
3. Dadashi-Silab S, Doran S, Yagci Y (2016) Photoinduced electron transfer reactions for macromolecular syntheses. Chem Rev 116(17):10212–10275
4. D'Souza F, Ito O (2012) Photosensitized electron transfer processes of nanocarbons applicable to solar cells. Chem Soc Rev 41(1):86–96
5. Liu Z, Qi W, Xu G (2015) Recent advances in electrochemiluminescence. Chem Soc Rev 44(10):3117–3142

6. Lou Z, Li P, Han K (2015) Redox-responsive fluorescent probes with different design strategies. Acc Chem Res 48(5):1358–1368
7. Banyasz A, Ketola T-M, Muñoz-Losa A, Rishi S, Adhikary A, Sevilla MD, Martinez-Fernandez L, Improta R, Markovitsi D (2016) UV-induced adenine radicals induced in DNA A-tracts: spectral and dynamical characterization. J Phys Chem Lett 7(19):3949–3953
8. Marguet S, Markovitsi D, Talbot F (2006) One- and two-photon ionization of DNA single and double helices studied by laser flash photolysis at 266 nm. J Phys Chem B 110(23):11037–11039
9. Crespo-Hernández CE, Arce R (2003) Near threshold photo-oxidation of dinucleotides containing purines upon 266 nm nanosecond laser excitation. The role of base stacking, conformation, and sequence. J Phys Chem B 107(4):1062–1070
10. Banyasz A, Martínez-Fernández L, Balty C, Perron M, Douki T, Improta R, Markovitsi D (2017) Absorption of low-energy UV radiation by human telomere G-quadruplexes generates long-lived guanine radical cations. J Am Chem Soc 139(30):10561–10568
11. Banyasz A, Ketola T-MC, Martinez-Fernandez L, Improta R, Markovitsi D (2017) Adenine radicals generated in alternating AT duplexes by direct absorption of low-energy UV radiation. Faraday Discuss
12. Schroeder CA, Pluhařová E, Seidel R, Schroeder WP, Faubel M, Slavicek P, Winter B, Jungwirth P, Bradforth SE (2015) Oxidation half-reaction of aqueous nucleosides and nucleotides via photoelectron spectroscopy augmented by ab initio calculations. J Am Chem Soc 137(1):201–209
13. Martinez-Fernandez L, Zhang Y, de La Harpe K, Beckstead AA, Kohler B, Improta R (2016) Photoinduced long-lived charge transfer excited states in AT-DNA strands. Phys Chem Chem Phys 18(31):21241–21245
14. Zhang Y, de La Harpe K, Beckstead AA, Improta R, Kohler B (2015) UV-induced proton transfer between DNA strands. J Am Chem Soc 137(22):7059–7062
15. Zhang Y, de La Harpe K, Beckstead AA, Martínez-Fernández L, Improta R, Kohler B (2016) Excited-state dynamics of DNA duplexes with different H-bonding motifs. J Phys Chem Lett 7(6):950–954
16. Zhang Y, Dood J, Beckstead AA, Li XB, Nguyen KV, Burrows CJ, Improta R, Kohler B (2014) Efficient UV-induced charge separation and recombination in an 8-oxoguanine-containing dinucleotide. Proc Natl Acad Sci 111(32):11612–11617
17. Bucher DB, Pilles BM, Carell T, Zinth W (2014) Charge separation and charge delocalization identified in long-living states of photoexcited DNA. Proc Natl Acad Sci 111(12):4369–4374
18. Pilles BM, Bucher DB, Liu LZ, Gilch P, Zinth W, Schreier WJ (2014) Identification of charge separated states in thymine single strands. Chem Commun 50(98):15623–15626
19. Doorley GW, McGovern DA, George MW, Towrie M, Parker AW, Kelly JM, Quinn SJ (2009) Picosecond transient infrared study of the ultrafast deactivation processes of electronically Excited B-DNA and Z-DNA forms of $[poly(dG\text{-}dC)]_2$. Ang Chem Int Ed 48(1):123–127
20. Doorley GW, Wojdyla M, Watson GW, Towrie M, Parker AW, Kelly JM, Quinn SJ (2013) Tracking DNA excited states by picosecond-time-resolved infrared spectroscopy: signature band for a charge-transfer excited state in stacked adenine-thymine systems. J Phys Chem Lett 4(16):2739–2744
21. Keane PM, Wojdyla M, Doorley GW, Kelly JM, Parker AW, Clark IP, Greetham GM, Towrie M, Magno LM, Quinn SJ (2014) Long-lived excited states in i-motif DNA studied by picosecond time-resolved IR spectroscopy. Chem Commun 50(23):2990–2992
22. Kawai K, Majima T (2013) Hole transfer kinetics of DNA. Acc Chem Res 46(11):2616–2625
23. Vura-Weis J, Wasielewski MR, Thazhathveetil AK, Lewis FD (2009) Efficient charge transport in DNA diblock oligomers. J Am Chem Soc 131(28):9722–9727
24. Renaud N, Harris MA, Singh APN, Berlin YA, Ratner MA, Wasielewski MR, Lewis FD, Grozema FC (2016) Deep-hole transfer leads to ultrafast charge migration in DNA hairpins. Nat Chem 8:1015
25. Slinker JD, Muren NB, Renfrew SE, Barton JK (2011) DNA charge transport over 34 nm. Nat Chem 3(3):228–233
26. Choi J, Park J, Tanaka A, Park MJ, Jang YJ, Fujitsuka M, Kim SK, Majima T (2013) Hole trapping of G-quartets in a G-quadruplex. Ang Chem Int Ed 52(4):1134–1138
27. Thazhathveetil AK, Harris MA, Young RM, Wasielewski MR, Lewis FD (2017) Efficient charge transport via DNA G-quadruplexes. J Am Chem Soc 139(5):1730–1733
28. Roca-Sanjuán D, Merchán M, Serrano-Andrés L (2008) Modeling hole transfer in DNA: low-lying excited states of oxidized cytosine homodimer and cytosine–adenine heterodimer. Chem Phys 349(1):188–196
29. Arnold Anna R, Grodick Michael A, Barton Jacqueline K (2016) DNA charge transport: from chemical principles to the cell. Cell Chem Biol 23(1):183–197
30. Genereux JC, Barton JK (2010) Mechanisms for DNA charge transport. Chem Rev 110(3):1642–1662
31. Wagenknecht H-A (ed) (2006) Charge transfer in DNA: from mechanism to application. Wiley-VCH, Weinheim
32. Hall DB, Holmlin RE, Barton JK (1996) Oxidative DNA damage through long-range electron transfer. Nature 382:731
33. Murphy CJ, Arkin MR, Jenkins Y, Ghatlia ND, Bossmann SH, Turro NJ, Barton JK (1993) Long-range photoinduced electron transfer through a DNA helix. Science 262(5136):1025
34. Adhikary A, Khanduri D, Sevilla MD (2009) Direct observation of the hole protonation state and hole localization site in DNA-oligomers. J Am Chem Soc 131(24):8614–8619
35. Adhikary A, Kumar A, Khanduri D, Sevilla MD (2008) Effect of base stacking on the acid–base properties of the adenine cation radical [A· +] in solution: ESR and DFT studies. J Am Chem Soc 130(31):10282–10292
36. Kumar A, Sevilla MD (2011) Density functional theory studies of the extent of hole delocalization in one-electron oxidized adenine and guanine base stacks. J Phys Chem B 115(17):4990–5000
37. Lewis FD, Liu X, Liu J, Miller SE, Hayes RT, Wasielewski MR (2000) Direct measurement of hole transport dynamics in DNA. Nature 406:51
38. Capobianco A, Caruso T, Peluso A (2015) Hole delocalization over adenine tracts in single stranded DNA oligonucleotides. Phys Chem Chem Phys 17(6):4750–4756
39. Capobianco A, Peluso A (2014) The oxidization potential of AA steps in single strand DNA oligomers. RSC Adv 4(88):47887–47893
40. Capobianco A, Caruso T, D'Ursi AM, Fusco S, Masi A, Scrima M, Chatgilialoglu C, Peluso A (2015) Delocalized hole domains in guanine-rich DNA oligonucleotides. J Phys Chem B 119(17):5462–5466
41. Capobianco A, Caruso T, Celentano M, D'Ursi AM, Scrima M, Peluso A (2013) Stacking interactions between adenines in oxidized oligonucleotides. J Phys Chem B 117(30):8947–8953
42. Adhikary A, Khanduri D, Kumar A, Sevilla MD (2008) Photoexcitation of Adenine cation radical [A·(+)] in the near UV–Vis region produces sugar radicals in Adenosine and in its nucleotides. J Phys Chem B 112(49):15844–15855
43. Candeias LP, Steenken S (1992) Ionization of purine nucleosides and nucleotides and their components by 193-nm laser photolysis in aqueous solution: model studies for oxidative damage of DNA. J Am Chem Soc 114(2):699–704

44. von Sonntag C (2006) Free-radical-induced DNA damage and its repair. Springer, Berlin
45. Becke AD (1993) Density-functional thermochemistry. III. The role of exact exchange. J Chem Phys 98(7):5648–5652
46. Yanai T, Tew DP, Handy NC (2004) A new hybrid exchange-correlation functional using the Coulomb-attenuating method (CAM-B3LYP). Chem Phys Lett 393(1–3):51–57
47. Zhao Y, Schultz NE, Truhlar DG (2006) Design of density functionals by combining the method of constraint satisfaction with parametrization for thermochemistry, thermochemical kinetics, and noncovalent interactions. J Chem Theor Comput 2(2):364–382
48. Zhao Y, Truhlar DG (2008) Density functionals with broad applicability in chemistry. Acc Chem Res 41(2):157–167
49. Miertuš S, Scrocco E, Tomasi J (1981) Electrostatic interaction of a solute with a continuum. A direct utilization of AB initio molecular potentials for the prevision of solvent effects. Chem Phys 55:117–129
50. Tomasi J, Mennucci B, Cammi R (2005) Quantum mechanical continuum solvation models. Chem Rev 105(8):2999–3093
51. Improta R, Scalmani G, Frisch MJ, Barone V (2007) Toward effective and reliable fluorescence energies in solution by a new state specific polarizable continuum model time dependent density functional theory approach. J Chem Phys 127(7):074504
52. Pluhařová E, Jungwirth P, Bradforth SE, Slavíček P (2011) Ionization of purine tautomers in nucleobases, nucleosides, and nucleotides: from the gas phase to the aqueous environment. J Phys Chem B 115(5):1294–1305
53. Muñoz-Losa A, Markovitsi D, Improta R (2015) A state-specific PCM–DFT method to include dynamic solvent effects in the calculation of ionization energies: application to DNA bases. Chem Phys Lett 634(Supplement C):20–24
54. Frisch MJ et al (2009) Gaussian 09, revision A.1. Gaussian, Inc.,Wallingford
55. Lavery R, Zakrzewska K, Sklenar H (1995) JUMNA (junction minimisation of nucleic acids). Comput Phys Commun 91(1):135–158
56. Case DA, Darden TA, Cheatham TE, Simmerling CL, Wang J, Duke RE, Luo R, Walker RC, Zhang W, Merz KM, Roberts B, Wang B, Hayik S, Roitberg A, Seabra G, Kolossváry I, Wong KF, Paesani F, Vanicek J, Liu J, Wu X, Brozell SR, Steinbrecher T, Gohlke H, Cai Q, Ye X, Wang J, Hsieh MJ, Cui G, Roe DR, Mathews DH, Seetin MG, Sagui C, Babin V, Luchko T, Gusarov S, Kovalenko A, Kollman PA (2010) AMBER 11. University of California, San Francisco
57. Pérez A, Marchán I, Svozil D, Sponer J, Cheatham TE, Laughton CA, Orozco M (2007) Refinement of the AMBER force field for nucleic acids: improving the description of α/γ conformers. Biophys J 92(11):3817–3829
58. Wang J, Cieplak P, Kollman PA (2000) How well does a restrained electrostatic potential (RESP) model perform in calculating conformational energies of organic and biological molecules? J Comput Chem 21(12):1049–1074
59. Berendsen HJC, Grigera JR, Straatsma TP (1987) The missing term in effective pair potentials. J Phys Chem 91(24):6269–6271
60. Lavery R, Zakrzewska K, Beveridge D, Bishop TC, Case DA, Cheatham T, Dixit S, Jayaram B, Lankas F, Laughton C, Maddocks JH, Michon A, Osman R, Orozco M, Perez A, Singh T, Spackova N, Sponer J (2010) A systematic molecular dynamics study of nearest-neighbor effects on base pair and base pair step conformations and fluctuations in B-DNA. Nucl Acids Res 38(1):299–313
61. Esposito L, Banyasz A, Douki T, Perron M, Markovitsi D, Improta R (2014) Effect of C5-methylation of cytosine on the photoreactivity of DNA: a joint experimental and computational study of TCG trinucleotides. J Am Chem Soc 136:10838–10841
62. Dixit SB, Beveridge DL, Case DA, Cheatham TE, Giudice E, Lankas F, Lavery R, Maddocks JH, Osman R, Sklenar H, Thayer KM, Varnai P (2005) Molecular dynamics simulations of the 136 unique tetranucleotide sequences of DNA oligonucleotides. II: sequence context effects on the dynamical structures of the 10 unique dinucleotide steps. Biophys J 89(6):3721–3740
63. Ryckaert J-P, Ciccotti G, Berendsen HJC (1977) Numerical integration of the cartesian equations of motion of a system with constraints: molecular dynamics of n-alkanes. J Comput Phys 23(3):327–341
64. Pluhařová E, Slavicek P, Jungwirth P (2015) Modeling photoionization of aqueous DNA and its components. Acc Chem Res 48(5):1209–1217
65. Roca-Sanjuán D, Rubio M, Merchán M, Serrano-Andrés L (2006) Ab initio determination of the ionization potentials of DNA and RNA nucleobases. J Chem Phys 125(8):084302
66. Barbatti M, Ullrich S (2011) Ionization potentials of adenine along the internal conversion pathways. Phys Chem Chem Phys 13(34):15492–15500
67. Improta R, Barone V, Scalmani G, Frisch MJ (2006) A state-specific polarizable continuum model time dependent density functional theory method for excited state calculations in solution. J Chem Phys 125:054103
68. Pluhařová E, Schroeder C, Seidel R, Bradforth SE, Winter B, Faubel M, Slavíček P, Jungwirth P (2013) Unexpectedly small effect of the DNA environment on vertical ionization energies of aqueous nucleobases. J Phys Chem Lett 4(21):3766–3769
69. Ferrer FJA, Cerezo J, Stendardo E, Improta R, Santoro F (2013) Insights for an accurate comparison of computational data to experimental absorption and emission spectra: beyond the vertical transition approximation. J Chem Theor Comput 9(4):2072–2082
70. Avila Ferrer FJ, Cerezo J, Soto J, Improta R, Santoro F (2014) First-principle computation of absorption and fluorescence spectra in solution accounting for vibronic structure, temperature effects and solvent inhomogeneous broadening. Comput Theor Chem 1040–1041(Supplement C):328–337
71. Dreuw A, Head-Gordon M (2005) Single-reference ab initio methods for the calculation of excited states of large molecules. Chem Rev 105(11):4009–4037
72. Donati G, Lingerfelt DB, Petrone A, Rega N, Li X (2016) "Watching" polaron pair formation from first-principles electron-nuclear dynamics. J Phys Chem A 120(37):7255–7261